International Journal of Recent Technology and Engineering (IJRTE)
ISSN: 2277-3878 (Online), Volume-14 Issue-1, May 2025

Three-Dimensional Position-Measuring Instrument using Two Manipulators

Hirofumi Maeda

Abstract*: In Japan, the number of sewer culverts with a service life of 50 years has increased, and ageing facilities have become apparent. In recent years, therefore, robots have been used for pipe inspections. Thus, the robot must grasp the situation and perform actions to prevent tipping over in the pipe. Consequently, we have decided to explore a software approach to prevent tipping using driving control, aiming to achieve highly accurate self-position estimation, which is necessary for this approach to be practical. Although we have established a basic localisation method based on our previous research, a small estimation error remains due to the influence of tire shape. Therefore, we propose a highly accurate localisation method that utilises a neural network to compensate for this estimation error. However, a large amount of teacher data was required to achieve this. For this reason, this research develops a three-dimensional position-measuring instrument that can quickly perform many measurements with high accuracy using two commercially available manipulators. This paper presents a three-dimensional position-measuring machine that can quickly perform high-precision and high-volume measurements using two commercially available manipulators. The paper demonstrates how to connect two manipulators utilising a ball joint and proposes a highly accurate measurement theory utilising an IMU. Furthermore, we confirm that the accuracy of the contact-type three-dimensional position-measuring is within 1 mm on average for translation error, within 1 deg on average for angular error, within 1 mm for the standard deviation of translation error, and 1 deg for the standard deviation of angular error except for ${}^{0}\gamma_{p3}$, even in the initial state without calibration. This result shows that the method can be used in a neural network to correct estimation errors.

***Keywords*: Measuring Instrument, Manipulator, Contact Type, Exploration Robot, Water Pipe**

Abbreviations:
AMU: Attitude Measurement Unit
CPU: Central Processing Unit
GPU: Graphics Processing Unit
OS: Operating System
IMU: Inertial Measurement Unit

I. INTRODUCTION

In Japan, the number of sewer culverts with a service life of 50 years has increased, and ageing facilities have become apparent. In particular, problems such as sewer pipe caving Rainwater spills caused by heavy rains have become a concern, so local governments conduct detailed inspections and partially repair problem areas. However, these tasks are too work, time-consuming, and labour-intensive for humans.

In recent years, therefore, robots have come to be used for pipe inspections [1]. Robots can be broadly classified into two types: remotely operated and stand-alone [2]. In the remotely operated type, the robot is controlled via a wired system from a ground-based transport vehicle. This method enables the operator to control and monitor the robot in real-time, allowing it to respond effectively to unforeseen situations. Additionally, the robot's power supply, control unit, and other components can be mounted on the transport vehicle, thereby reducing the robot's main body weight and enhancing its operability. However, installing the transport vehicle requires time and money for inspections, such as securing the site and restricting traffic at the work site. On the other hand, a stand-alone robot can be inspected quickly by a small number of people [3]. However, the development of stand-alone robots in Japan has not been active, and most of the robots developed overseas are designed for pipe diameters of 200 mm or more, which is often not applicable in Japan, where most pipes are 150 mm in diameter [4].

Against this background, we have conducted extensive research and development on the practical application of compact and easily transportable stand-alone robots [5]. The inside pipe to be inspected allows the robot to tip over due to external disturbances, such as steps caused by joints between pipes, sinking due to ageing, sludge, etc. Therefore, the robot must grasp the situation and perform actions to prevent tipping over in the pipe [6]. Many robots have taken measures to prevent tipping over, such as adjusting the shape of their tires and the distance between their axes. However, while these hardware-based countermeasures can prevent tipping, they cannot completely stop it. Therefore, we have decided to explore a software approach to prevent tipping using driving control and aim to realize highly accurate self-position estimation, which is necessary for this approach [7].

Although we have established a basic localization method based on our previous research, there is a small estimation error due to the influence of tire shape [8]. Therefore, we propose a highly accurate localization method using a neural network to compensate for this estimation error [9]. However, a large amount of teacher data was required to achieve this. In addition, a unique three-dimensional position-measuring instrument for a piping inspection robot used for accuracy verification requires a significant amount of time for each data acquisition to obtain accurate position information. Therefore, It is unsuitable for use in neural networks [10]. For this

Manuscript received on 07 February 2025 | First Revised Manuscript received on 12 February 2025 | Second Revised Manuscript received on 16 April 2025 | Manuscript Accepted on 15 May 2025 | Manuscript published on 30 May 2025.
*Correspondence Author(s)
Prof. Hirofumi Maeda*, Department of Information Science and Technology, National Institute of Technology (KOSEN), Yuge College, Ehime Prefecture, Japan. Email ID: maeda@info.yuge.ac.jp, ORCID ID: 0000-0002-7145-3889.

reason, this research develops a three-dimensional position-measuring instrument that can quickly perform many measurements with high accuracy using two commercially available manipulators.

II. THREE-DIMENSIONAL POSITION-MEASURING INSTRUMENT

Figure 1 shows the contact-type three-dimensional position-measuring instrument. A test field with a pipe cut in half, as shown in Figure 2, is placed in the centre of the instrument, and a previously fabricated verification robot is used to acquire the teacher data. Fig. 1 shows a 6-axis stage installed in the centre of the instrument for accuracy verification. Following the guidelines in the surrounding area, this stage can be easily replaced with the test field. The structure of the instrument and system configuration are described below.

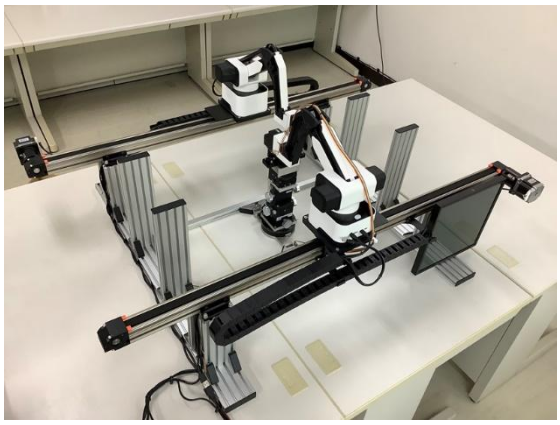

[Fig.1: Contact-Type Three-Dimensional Position-Measuring Instrument]

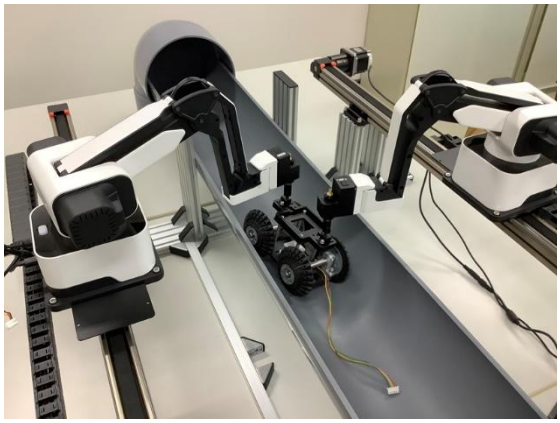

[Fig.2: Measuring Instrument during Acquisition of Teacher Data]

A. Measuring Instrument Structure

Figure 3 shows the measuring instrument using two DexArm manipulators from Rotrics. The DexArm has four degrees of freedom and can be used for various applications by changing the modules attached to the end-effectors. Additionally, the working area is 220 x 220 x 270 mm with an accuracy of 0.1 mm and repeatability of 0.5 mm.

Figure 4 shows the link structure of the DexArm. The DexArm has four degrees of freedom, including the degrees of freedom of the end-effector attached to the tip, and the manipulator part has three degrees of freedom, as shown in Figure 4. The position information of the end-effector, which is the tip of the manipulator, is provided with an acquisition function in advance and does not need to be calculated using forward kinematics based on the encoder values. Furthermore, the DexArm features a direct teaching function, enabling users to acquire encoder values while the motor is turned off. In this system, the DexArm is used as the measuring instrument in direct teaching mode.

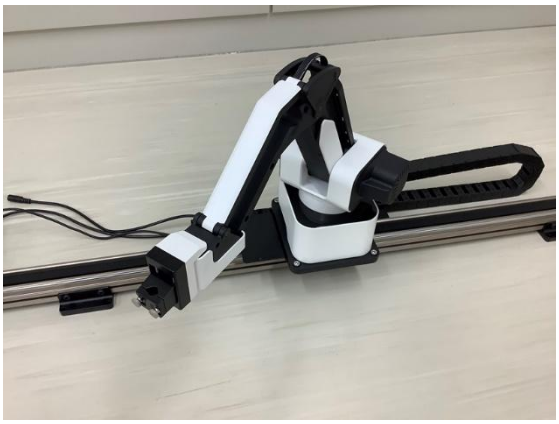

[Fig.3: DexArm Manufactured by Rotrics]

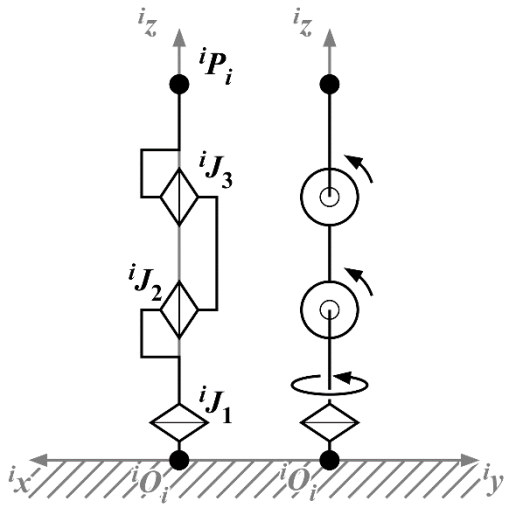

i : manipulator number (i = 1, 2)
$^iJ_3$ - $^iJ_3$: the position of each joint
^iP_i : the position of the end effector

[Fig.4: Link Structure of DexArm]

Each manipulator is fixed on top of Rotrics' Sliding Rail Kit, and the two Sliding Rail Kits and the test field are installed to be parallel. The Sliding Rail Kit is fixed in this study and is not driven.

Next, the module connecting the end-effectors of the two manipulators is described. The manipulators can freely change the position of the end-effectors, but their posture is fixed, ensuring they always face straight down. Therefore, the commercially available pneumatic suction cup shown on the left in Figure 5 is modified as shown on the right and attached to the connection component shown in Figure 6. This results in two manipulators being connected via a ball joint, and the position and posture of the connecting part, which serves

as the measuring point, can be freely adjusted.

A previous study found that the acceleration values of AMU-3002B Lite (Silicon Sensing Systems Japan, Inc.), an An IMU mounted on a piping inspection robot can accurately measure the robot's roll and yaw directions, which are also used in this measurement. However, since AMU-3002B Lite is not mounted on the 6-axis stage used for accuracy verification, it is installed on top of the module, as shown in Figure 7.

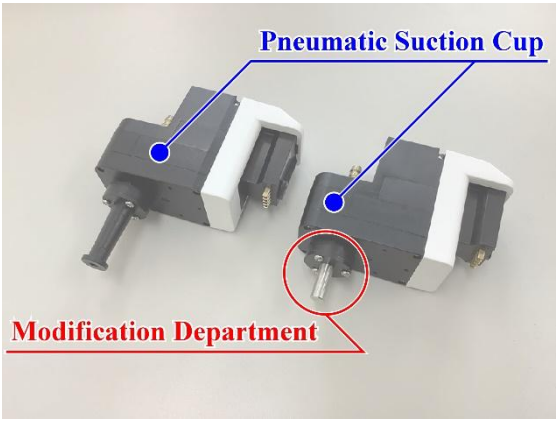

[Fig.5: Pneumatic Suction Cup]

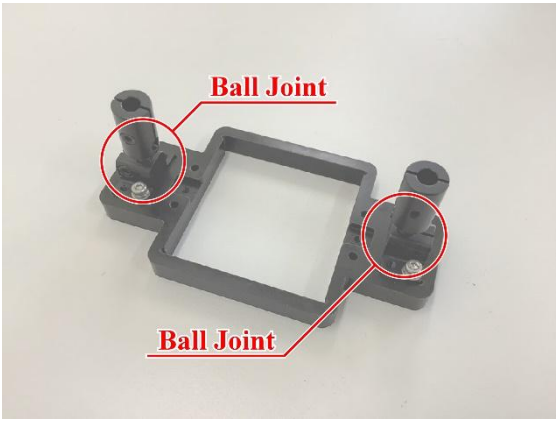

[Fig.6: Connecting Part]

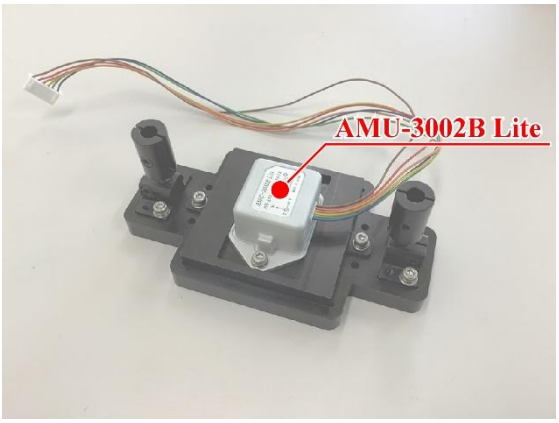

[Fig.7: Connecting Module with IMU]

B. System Configuration

Figure 8 shows a schematic diagram of the system. Two DexArms are connected to a PC via USB to obtain end-effector position information in direct teaching mode, as described earlier. The AMU-3002B Lite, like the DexArm, sends acceleration information to the PC via USB. The PC processes this information using a program to calculate the position and posture of the measurement point. Note that Python is used for programming. Table-I shows the PC specifications. The calculation method is described in detail in the next chapter.

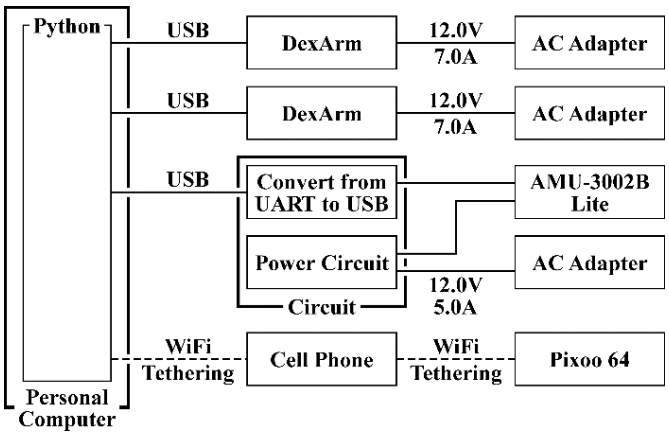

[Fig.8: Schematic Diagram of System]

Table-I: PC Specifications

Model Name	LEVEL-C066-LC127-SAX
Product Model Number	ILeDEs-C066-L127-SASXB
CPU	Intel Core i7-12700 Processor (4.90GHz / 12 core)
GPU	GeForce RTX 3060 Ti 8GB GDDR6
Memory	32GB (16GB×2) DDR4-3200
OS	Windows 11 Home (DSP)

Finally, to support accuracy verification, the calculated position and posture of the measurement points are sent to Divoom's Pixoo 64 via tethering on a cell phone, and the values are displayed as pixel art. Figure 9 shows the Pixoo 64 displaying the position and posture information.

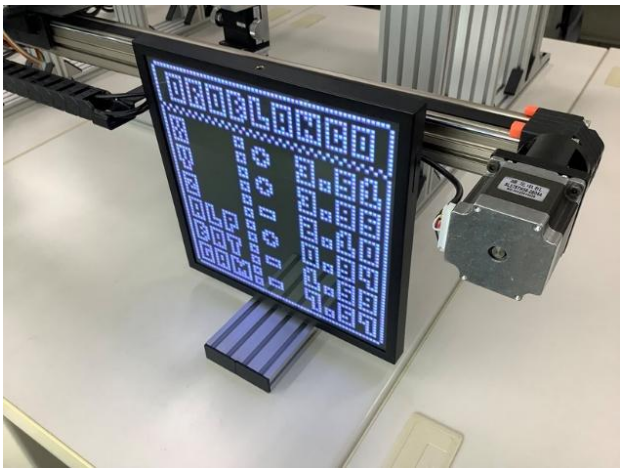

[Fig.9: Pixoo 64]

III. THEORY OF MEASUREMENT

Figure 10 shows the three-dimensional position-measuring instruments and their positional relationships. The two coordinate systems in Figure 10 are based on each manipulator's origins, ${}^{1}\boldsymbol{O}_1$ and ${}^{2}\boldsymbol{O}_2$. ${}^{1}\boldsymbol{P}_1$ and ${}^{2}\boldsymbol{P}_2$ represent the tip of the end-effector in the coordinate systems of manipulators 1 and 2. The coordinates around the

Published By:
Blue Eyes Intelligence Engineering
and Sciences Publication (BEIESP)

connection module are shown in Figure 11. In Fig. 11, ${}^0\boldsymbol{P_1}$ and ${}^0\boldsymbol{P_2}$ represent ${}^1\boldsymbol{P_1}$ and ${}^2\boldsymbol{P_2}$ in the absolute coordinate system, and the measurement point ${}^0\boldsymbol{P_3}$ is located 15.5 mm directly below the centre point connecting the two end-effector tips ${}^0\boldsymbol{P_1}$ and ${}^0\boldsymbol{P_2}$.

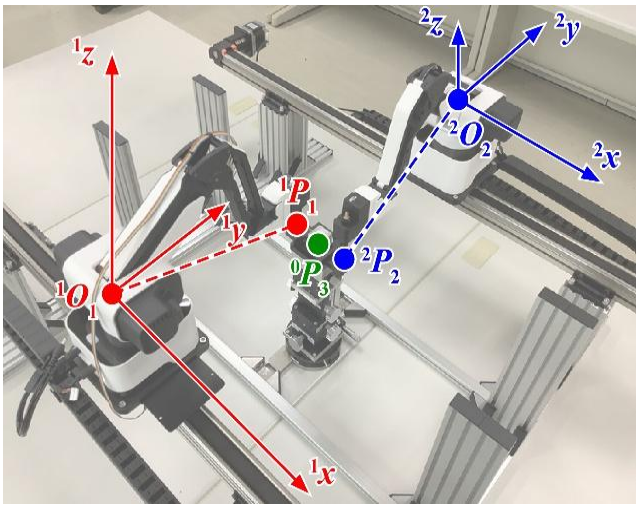

[Fig.10: Coordinate System of Measuring Instrument]

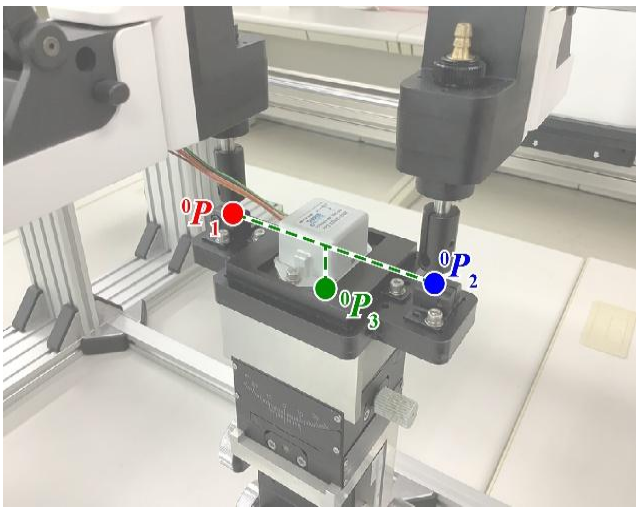

[Fig.11: Measuring Points of Measuring Instrument]

This section describes the position and posture of the measurement point ${}^0\boldsymbol{P_3}$ in the absolute coordinate system. First, define the origin ${}^0\boldsymbol{O_1}$, ${}^0\boldsymbol{O_2}$, ${}^0\boldsymbol{O_3}$ of each coordinate system in the absolute coordinate system, the tips ${}^0\boldsymbol{P_1}$, ${}^0\boldsymbol{P_2}$ of each end-effector, the measuring point ${}^0\boldsymbol{P_3}$, and the position and posture components of the measuring point ${}^0\boldsymbol{d}$ with the centre point of ${}^0\boldsymbol{P_1}$ and ${}^0\boldsymbol{P_2}$ as origin as follows. Therefore, equations can express each coordinate (1) to (7). Where ${}^0\boldsymbol{O_0}$ is the origin of the absolute coordinate system.

${}^0x_{o2}$: x-coordinate of the manipulator two origin ${}^0\boldsymbol{O_2}$ in the absolute coordinate system (m)
${}^0y_{o2}$: y-coordinate of the manipulator two origin ${}^0\boldsymbol{O_2}$ in the absolute coordinate system (m)
${}^0z_{o2}$: z-coordinate of the manipulator 2 origin ${}^0\boldsymbol{O_2}$ in the absolute coordinate system (m)
${}^0x_{o3}$: x-coordinate of the test field origin ${}^0\boldsymbol{O_3}$ in the absolute coordinate system (m)
${}^0y_{o3}$: y-coordinate of the test field origin ${}^0\boldsymbol{O_3}$ in the absolute coordinate system (m)
${}^0z_{o3}$: z-coordinate of the test field origin ${}^0\boldsymbol{O_3}$ in the absolute coordinate system (m)
${}^0x_{p1}$: x-coordinate of the manipulator 1 end-effector ${}^0\boldsymbol{P_1}$ in The absolute coordinate system (m)
${}^0y_{p1}$: y-coordinate of the manipulator 1 end-effector ${}^0\boldsymbol{P_1}$ in The absolute coordinate system (m)
${}^0z_{p1}$: z-coordinate of the manipulator 1 end-effector ${}^0\boldsymbol{P_1}$ in The absolute coordinate system (m)
${}^0\gamma_{p1}$: Yaw angle of the manipulator 1 end-effector ${}^0\boldsymbol{P_1}$ in The absolute coordinate system (rad)
${}^0x_{p2}$: x-coordinate of the manipulator 2 end-effector ${}^0\boldsymbol{P_2}$ in The absolute coordinate system (m)
${}^0y_{p2}$: y-coordinate of the manipulator 2 end-effector ${}^0\boldsymbol{P_2}$ in The absolute coordinate system (m)
${}^0z_{p2}$: z-coordinate of the manipulator 2 end-effector ${}^0\boldsymbol{P_2}$ in The absolute coordinate system (m)
${}^0\gamma_{p2}$: Yaw angle of the manipulator 2 end-effector ${}^0\boldsymbol{P_2}$ in The absolute coordinate system (rad)
${}^0x_{p3}$: x-coordinate of the measurement point in the absolute coordinate system (m)
${}^0y_{p3}$: y-coordinate of the measurement point in the absolute coordinate system (m)
${}^0z_{p3}$: z-coordinate of the measurement point in the absolute coordinate system (m)
${}^0\alpha_{p3}$: roll angle of the measurement point in the absolute coordinate system (rad)
${}^0\beta_{p3}$: Pitch angle of the measurement point in the absolute coordinate system (rad)
${}^0\gamma_{p3}$: Yaw angle of the measurement point in the absolute coordinate system (rad)
${}^0d_x$: x-coordinate of the measurement point in the absolute coordinate system with the origin at the centre point of ${}^0\boldsymbol{P_1}$ and ${}^0\boldsymbol{P_2}$ (m)
${}^0d_y$: y-coordinate of the measurement point in the absolute coordinate system with the origin at the centre point of ${}^0\boldsymbol{P_1}$ and ${}^0\boldsymbol{P_2}$ (m)
${}^0d_z$: z-coordinate of the measurement point in the absolute coordinate system with the origin at the centre point of ${}^0\boldsymbol{P_1}$ and ${}^0\boldsymbol{P_2}$ (m)

$$ {}^0\boldsymbol{O_1} = {}^0\boldsymbol{O_0} = (0, 0, 0, 0, 0, 0) \quad \ldots \quad (1) $$

$$ {}^0\boldsymbol{O_2} = \left({}^0x_{o2},\ {}^0y_{o2},\ {}^0z_{o2}, 0, 0, 0 \right) \quad \ldots \quad (2) $$

$$ {}^0\boldsymbol{O_3} = \left({}^0x_{o3},\ {}^0y_{o3},\ {}^0z_{o3}, 0, 0, 0 \right) \quad \ldots \quad (3) $$

$$ {}^0\boldsymbol{P_1} = \left({}^0x_{p1},\ {}^0y_{p1},\ {}^0z_{p1}, -\pi, 0,\ {}^0\gamma_{p1} \right) \quad \ldots \quad (4) $$

$$ {}^0\boldsymbol{P_2} = \left({}^0x_{p2},\ {}^0y_{p2},\ {}^0z_{p2}, -\pi, 0,\ {}^0\gamma_{p2} \right) \quad \ldots \quad (5) $$

$$ {}^0\boldsymbol{P}_3 = \left({}^0x_{p3},\ {}^0y_{p3},\ {}^0z_{p3},\ {}^0\alpha_{p3},\ {}^0\beta_{p3},\ {}^0\gamma_{p3} \right) \quad \ldots \quad (6) $$

$$ {}^0\boldsymbol{d} = \left({}^0d_x,\ {}^0d_y,\ {}^0d_z,\ {}^0\alpha_{p3}-\pi,\ {}^0\beta_{p3},\ {}^0\gamma_{p3} \right) \quad \ldots \quad (7) $$

Next, defining d_0 as in the Equation (8) allows Equation (7) to be expressed as Equation (9).

$$ d_0 = \sqrt{ {}^0d_x{}^2 + {}^0d_y{}^2 + {}^0d_z{}^2 } \quad \ldots \quad (8) $$

$$ {}^0\boldsymbol{d} = {}^0\boldsymbol{R}_\gamma \cdot {}^0\boldsymbol{R}_\beta \cdot {}^0\boldsymbol{R}_\alpha \begin{bmatrix} 0 \\ 0 \\ d_0 \end{bmatrix} $$

$$ = \begin{bmatrix} \cos {}^0\gamma_{p3} & -\sin {}^0\gamma_{p3} & 0 \\ \sin {}^0\gamma_{p3} & \cos {}^0\gamma_{p3} & 0 \\ 0 & 0 & 1 \end{bmatrix} \begin{bmatrix} \cos {}^0\beta_{p3} & 0 & \sin {}^0\beta_{p3} \\ 0 & 1 & 0 \\ -\sin {}^0\beta_{p3} & 0 & \cos {}^0\beta_{p3} \end{bmatrix} \begin{bmatrix} 1 & 0 & 0 \\ 0 & \cos {}^0\alpha_{p3} & -\sin {}^0\alpha_{p3} \\ 0 & \sin {}^0\alpha_{p3} & \cos {}^0\alpha_{p3} \end{bmatrix} \begin{bmatrix} 0 \\ 0 \\ d_0 \end{bmatrix} $$

$$ = \begin{bmatrix} d_0 \cos {}^0\alpha_{p3} \sin {}^0\beta_{p3} \cos {}^0\gamma_{p3} + d_0 \sin {}^0\alpha_{p3} \sin {}^0\gamma_{p3} \\ d_0 \cos {}^0\alpha_{p3} \sin {}^0\beta_{p3} \sin {}^0\gamma_{p3} - d_0 \sin {}^0\alpha_{p3} \cos {}^0\gamma_{p3} \\ d_0 \cos {}^0\alpha_{p3} \cos {}^0\beta_{p3} \end{bmatrix} \quad \ldots \quad (9) $$

Moreover, the measurement point ${}^0\boldsymbol{P}_3$ is converted to the coordinate system with the origin ${}^0\boldsymbol{O}_3$. In that case, the measurement point ${}^3\boldsymbol{P}_3$ can be defined by Equation (10), and the respective position components can be expressed by Equations (11) to (13).

$$ {}^3\boldsymbol{P}_3 = \left({}^3x_{p3},\ {}^3y_{p3},\ {}^3z_{p3},\ {}^0\alpha_{p3},\ {}^0\beta_{p3},\ {}^0\gamma_{p3} \right) \quad \ldots \quad (10) $$

$$ {}^3x_{p3} = {}^0x_{p1} + d_0 \cos {}^0\alpha_{p3} \sin {}^0\beta_{p3} \cos {}^0\gamma_{p3} + d_0 \sin {}^0\alpha_{p3} \sin {}^0\gamma_{p3} + \frac{ {}^0x_{p2} - {}^0x_{p1} }{2} - {}^0x_{o3} \quad \ldots \quad (11) $$

$$ {}^3y_{p3} = {}^0y_{p1} + d_0 \cos {}^0\alpha_{p3} \sin {}^0\beta_{p3} \sin {}^0\gamma_{p3} - d_0 \sin {}^0\alpha_{p3} \cos {}^0\gamma_{p3} + \frac{ {}^0y_{p2} - {}^0y_{p1} }{2} - {}^0y_{o3} \quad \ldots \quad (12) $$

$$ {}^3z_{p3} = {}^0z_{p1} + d_0 \cos {}^0\alpha_{p3} \cos {}^0\beta_{p3} + \frac{ {}^0z_{p2} - {}^0z_{p1} }{2} - {}^0z_{o3} \quad \ldots \quad (13) $$

The distance l between the axes connecting ${}^0\boldsymbol{P}_1$ and ${}^0\boldsymbol{P}_2$ is used to derive the attitude component. First, the relationship in Equation (14) holds for l. Furthermore, since ${}^0\boldsymbol{P}_1$ and ${}^0\boldsymbol{P}_2$ are on the x-axis in the initial state, Equation (15) is valid using Equation (14). Therefore, ${}^0\gamma_{p3}$ becomes equation (16).

$$ l = \sqrt{ \left({}^0x_{p2} - {}^0x_{p1} \right)^2 + \left({}^0y_{p2} - {}^0y_{p1} \right)^2 + \left({}^0z_{p2} - {}^0z_{p1} \right)^2 } \quad \ldots \quad (14) $$

$$ {}^0\boldsymbol{R}_\gamma \cdot {}^0\boldsymbol{R}_\beta \cdot {}^0\boldsymbol{R}_\alpha \begin{bmatrix} l \\ 0 \\ 0 \end{bmatrix} = \begin{bmatrix} \cos {}^0\gamma_{p3} & -\sin {}^0\gamma_{p3} & 0 \\ \sin {}^0\gamma_{p3} & \cos {}^0\gamma_{p3} & 0 \\ 0 & 0 & 1 \end{bmatrix} \begin{bmatrix} \cos {}^0\beta_{p3} & 0 & \sin {}^0\beta_{p3} \\ 0 & 1 & 0 \\ -\sin {}^0\beta_{p3} & 0 & \cos {}^0\beta_{p3} \end{bmatrix} \begin{bmatrix} 1 & 0 & 0 \\ 0 & \cos {}^0\alpha_{p3} & -\sin {}^0\alpha_{p3} \\ 0 & \sin {}^0\alpha_{p3} & \cos {}^0\alpha_{p3} \end{bmatrix} \begin{bmatrix} l \\ 0 \\ 0 \end{bmatrix} $$

$$ = \begin{bmatrix} l \cos {}^0\beta_{p3} \cos {}^0\gamma_{p3} \\ l \cos {}^0\beta_{p3} \sin {}^0\gamma_{p3} \\ -l \sin {}^0\beta_{p3} \end{bmatrix} = \begin{bmatrix} {}^0x_{p2} - {}^0x_{p1} \\ {}^0y_{p2} - {}^0y_{p1} \\ {}^0z_{p2} - {}^0z_{p1} \end{bmatrix} \quad \ldots \quad (15) $$

$$ \frac{ l \cos {}^0\beta_{p3} \sin {}^0\gamma_{p3} }{ l \cos {}^0\beta_{p3} \cos {}^0\gamma_{p3} } = \frac{ {}^0y_{p2} - {}^0y_{p1} }{ {}^0x_{p2} - {}^0x_{p1} } $$

$$ \frac{ \sin {}^0\gamma_{p3} }{ \cos {}^0\gamma_{p3} } = \frac{ {}^0y_{p2} - {}^0y_{p1} }{ {}^0x_{p2} - {}^0x_{p1} } $$

$$ \tan {}^0\gamma_{p3} = \frac{ {}^0y_{p2} - {}^0y_{p1} }{ {}^0x_{p2} - {}^0x_{p1} } $$

$$ {}^0\gamma_{p3} = \tan^{-1} \left(\frac{ {}^0y_{p2} - {}^0y_{p1} }{ {}^0x_{p2} - {}^0x_{p1} } \right) \quad \ldots \quad (16) $$

Finally, as described earlier, ${}^0\alpha_{p3}$ and ${}^0\beta_{p3}$ are derived using the acceleration values of AMU-3002B Lite, so Equations (17) and (18) are valid. The definitions of each variable are as follows.

- ${}^ra_x$: x component of the acceleration sensor in the robot coordinate system (m/s2)
- ${}^ra_y$: y component of the acceleration sensor in the robot coordinate system (m/s2)
- ${}^ra_z$: z component of the acceleration sensor in the robot coordinate system (m/s2)

$$ {}^0\alpha_{p3} = -\tan^{-1} \frac{ {}^ra_y }{ -{}^ra_z } \quad \ldots \quad (17) $$

$$ {}^0\beta_{p3} = -\tan^{-1} \frac{ -{}^ra_x }{ -{}^ra_z } \quad \ldots \quad (18) $$

IV. ACCURACY VERIFICATION

The accuracy of the contact-type three-dimensional position-measuring instrument was verified using a 6-axis stage. The accuracy verification was performed for both translation and rotation. For the accuracy verification in translation, the ${}^3\boldsymbol{P}_3$ ($^3x_{p3}$, $^3y_{p3}$,

${}^3z_{p3}$, ${}^0\alpha_{p3}$, ${}^0\beta_{p3}$, ${}^0\gamma_{p3}$) measurement points were used in the following: ${}^3x_{p3}$ = -20.0, 0.0, 20.0 mm; ${}^3y_{p3}$ = -20.0, 0.0, 20.0 mm; ${}^3z_{p3}$ = 0.0, 10.0, 20.0 mm; ${}^0\alpha_{p3} = {}^0\beta_{p3} = {}^0\gamma_{p3}$ = 0.0 deg in 27 patterns. Rotation was performed for 27 patterns of ${}^3x_{p3} = {}^3y_{p3} = {}^3z_{p3}$ = 0.0 mm, ${}^0\alpha_{p3}$ = -15.0, 0.0, 15.0 deg, ${}^0\beta_{p3}$ = -15.0, 0.0, 15.0 deg, and ${}^0\gamma_{p3}$ = -20.0, 0.0, 20.0 deg. The results of each experiment are shown in Table-II and Table-III.

Table II: Accuracy Verification Results in Translation

Ideal Value						Measured Value						Error					
${}^3x_{p3}$ [mm]	${}^3y_{p3}$ [mm]	${}^3z_{p3}$ [mm]	${}^3\alpha_{p3}$ [deg]	${}^3\beta_{p3}$ [deg]	${}^0\gamma_{p3}$ [deg]	${}^3x_{p3}$ [mm]	${}^3y_{p3}$ [mm]	${}^3z_{p3}$ [mm]	${}^3\alpha_{p3}$ [deg]	${}^3\beta_{p3}$ [deg]	${}^0\gamma_{p3}$ [deg]	${}^3x_{p3}$ [mm]	${}^3y_{p3}$ [mm]	${}^3z_{p3}$ [mm]	${}^3\alpha_{p3}$ [deg]	${}^3\beta_{p3}$ [deg]	${}^0\gamma_{p3}$ [deg]
-20.00	-20.00	0.00	0.00	0.00	0.00	-21.36	-20.41	-0.20	-0.44	0.47	0.22	-1.36	-0.41	-0.20	-0.44	0.47	0.22
-20.00	-20.00	10.00	0.00	0.00	0.00	-21.15	-20.81	9.85	-0.43	0.49	0.17	-1.15	-0.81	-0.15	-0.43	0.49	0.17
-20.00	-20.00	20.00	0.00	0.00	0.00	-21.36	-20.95	20.06	-0.43	0.50	0.30	-1.36	-0.95	0.06	-0.43	0.50	0.30
0.00	-20.00	0.00	0.00	0.00	0.00	-0.81	-20.99	0.18	-0.43	0.61	-0.19	-0.81	-0.99	0.18	-0.43	0.61	-0.19
0.00	-20.00	10.00	0.00	0.00	0.00	-1.45	-20.98	9.81	-0.43	0.49	0.29	-1.45	-0.98	-0.19	-0.43	0.49	0.29
0.00	-20.00	20.00	0.00	0.00	0.00	-0.56	-21.06	19.88	-0.43	0.58	0.11	-0.56	-1.06	-0.12	-0.43	0.58	0.11
20.00	-20.00	0.00	0.00	0.00	0.00	19.22	-20.04	-0.96	-0.43	0.69	1.56	-0.78	-0.04	-0.96	-0.43	0.69	1.56
20.00	-20.00	10.00	0.00	0.00	0.00	17.97	-20.94	9.85	-0.36	0.56	0.17	-2.03	-0.94	-0.15	-0.36	0.56	0.17
20.00	-20.00	20.00	0.00	0.00	0.00	18.62	-21.08	19.72	-0.36	0.64	0.30	-1.38	-1.08	-0.28	-0.36	0.64	0.30
-20.00	0.00	0.00	0.00	0.00	0.00	-21.48	-0.06	-0.14	-0.44	0.46	0.28	-1.48	-0.06	-0.14	-0.44	0.46	0.28
-20.00	0.00	10.00	0.00	0.00	0.00	-21.23	-0.46	9.73	-0.43	0.49	0.71	-1.23	-0.46	-0.27	-0.43	0.49	0.71
-20.00	0.00	20.00	0.00	0.00	0.00	-21.26	-0.51	19.72	-0.43	0.50	0.35	-1.26	-0.51	-0.28	-0.43	0.50	0.35
0.00	0.00	0.00	0.00	0.00	0.00	-1.08	-0.66	-0.46	-0.44	0.59	0.89	-1.08	-0.66	-0.46	-0.44	0.59	0.89
0.00	0.00	10.00	0.00	0.00	0.00	-1.06	-0.98	10.00	-0.43	0.50	0.10	-1.06	-0.98	0.00	-0.43	0.50	0.10
0.00	0.00	20.00	0.00	0.00	0.00	-1.08	-1.05	19.65	-0.42	0.58	0.46	-1.08	-1.05	-0.35	-0.42	0.58	0.46
20.00	0.00	0.00	0.00	0.00	0.00	19.98	-0.76	-0.38	-0.43	0.69	0.80	-0.02	-0.76	-0.38	-0.43	0.69	0.80
20.00	0.00	10.00	0.00	0.00	0.00	19.35	-0.91	10.07	-0.43	0.64	0.08	-0.65	-0.91	0.07	-0.43	0.64	0.08
20.00	0.00	20.00	0.00	0.00	0.00	19.33	-1.34	19.84	-0.43	0.64	0.53	-0.67	-1.34	-0.16	-0.43	0.64	0.53
-20.00	20.00	0.00	0.00	0.00	0.00	-20.24	18.86	-0.55	-0.44	0.47	0.73	-0.24	-1.14	-0.55	-0.44	0.47	0.73
-20.00	20.00	10.00	0.00	0.00	0.00	-20.27	19.45	9.58	-0.43	0.49	0.26	-0.27	-0.55	-0.42	-0.43	0.49	0.26
-20.00	20.00	20.00	0.00	0.00	0.00	-20.71	19.35	19.88	-0.43	0.50	0.14	-0.71	-0.65	-0.12	-0.43	0.50	0.14
0.00	20.00	0.00	0.00	0.00	0.00	-0.41	20.24	-0.52	-0.43	0.62	0.82	-0.41	0.24	-0.52	-0.43	0.62	0.82
0.00	20.00	10.00	0.00	0.00	0.00	-0.85	19.86	9.92	-0.43	0.56	0.26	-0.85	-0.14	-0.08	-0.43	0.56	0.26
0.00	20.00	20.00	0.00	0.00	0.00	-0.15	19.13	19.82	-0.43	0.57	0.27	-0.15	-0.87	-0.18	-0.43	0.57	0.27
20.00	20.00	0.00	0.00	0.00	0.00	20.48	20.60	-0.65	-0.43	0.69	1.51	0.48	0.60	-0.65	-0.43	0.69	1.51
20.00	20.00	10.00	0.00	0.00	0.00	19.44	18.80	9.86	-0.43	0.63	0.30	-0.56	-1.20	-0.14	-0.43	0.63	0.30
20.00	20.00	20.00	0.00	0.00	0.00	20.55	19.15	19.73	-0.43	0.64	0.69	0.55	-0.85	-0.27	-0.43	0.64	0.69
								average of error				-0.80	-0.69	-0.25	-0.43	0.57	0.45
								standard deviation of error				0.60	0.47	0.24	0.02	0.08	0.41

Table-III: Accuracy Verification Results for Rotation

Ideal Value						Measured Value						Error					
${}^3x_{p3}$ [mm]	${}^3y_{p3}$ [mm]	${}^3z_{p3}$ [mm]	${}^3\alpha_{p3}$ [deg]	${}^3\beta_{p3}$ [deg]	${}^0\gamma_{p3}$ [deg]	${}^3x_{p3}$ [mm]	${}^3y_{p3}$ [mm]	${}^3z_{p3}$ [mm]	${}^3\alpha_{p3}$ [deg]	${}^3\beta_{p3}$ [deg]	${}^0\gamma_{p3}$ [deg]	${}^3x_{p3}$ [mm]	${}^3y_{p3}$ [mm]	${}^3z_{p3}$ [mm]	${}^3\alpha_{p3}$ [deg]	${}^3\beta_{p3}$ [deg]	${}^0\gamma_{p3}$ [deg]
0.00	0.00	0.00	-15.00	-15.00	-20.00	-0.82	-0.93	-0.35	-16.05	-14.59	-15.46	-0.82	-0.93	-0.35	-1.05	0.41	4.54
0.00	0.00	0.00	-15.00	-15.00	0.00	-1.15	-1.15	0.31	-15.96	-14.58	4.08	-1.15	-1.15	0.31	-0.96	0.42	4.08
0.00	0.00	0.00	-15.00	-15.00	20.00	-1.00	-0.63	0.27	-15.96	-14.57	23.76	-1.00	-0.63	0.27	-0.96	0.43	3.76
0.00	0.00	0.00	0.00	-15.00	-20.00	-1.19	-0.93	-0.31	-0.45	-14.46	-19.51	-1.19	-0.93	-0.31	-0.45	0.54	0.49
0.00	0.00	0.00	0.00	-15.00	0.00	-1.17	-0.57	-0.17	-0.45	-14.46	0.44	-1.17	-0.57	-0.17	-0.45	0.54	0.44
0.00	0.00	0.00	0.00	-15.00	20.00	-2.20	-0.86	0.52	-0.45	-16.15	21.05	-2.20	-0.86	0.52	-0.45	-1.15	1.05
0.00	0.00	0.00	15.00	-15.00	-20.00	-0.28	-0.30	-0.28	15.58	-14.55	-23.63	-0.28	-0.30	-0.28	0.58	0.45	-3.63
0.00	0.00	0.00	15.00	-15.00	0.00	-0.86	-0.50	-0.15	15.58	-14.62	-3.48	-0.86	-0.50	-0.15	0.58	0.38	-3.48
0.00	0.00	0.00	15.00	-15.00	20.00	-1.30	-0.15	-0.33	15.58	-14.63	16.34	-1.30	-0.15	-0.33	0.58	0.37	-3.66
0.00	0.00	0.00	-15.00	0.00	-20.00	0.28	-0.27	-0.28	-15.70	0.41	-18.93	0.28	-0.27	-0.28	-0.70	0.41	1.07
0.00	0.00	0.00	-15.00	0.00	0.00	-1.18	-0.76	-0.41	-15.62	0.39	1.10	-1.18	-0.76	-0.41	-0.62	0.39	1.10
0.00	0.00	0.00	-15.00	0.00	20.00	-1.60	-0.75	-0.11	-15.62	0.41	20.64	-1.60	-0.75	-0.11	-0.62	0.41	0.64
0.00	0.00	0.00	0.00	0.00	-20.00	-0.39	-0.80	-0.58	-0.42	0.51	-19.51	-0.39	-0.80	-0.58	-0.42	0.51	0.49
0.00	0.00	0.00	0.00	0.00	0.00	-1.04	-0.59	-0.18	-0.42	0.44	0.49	-1.04	-0.59	-0.18	-0.42	0.44	0.49
0.00	0.00	0.00	0.00	0.00	20.00	-1.79	-0.69	-0.01	-0.42	0.44	20.02	-1.79	-0.69	-0.01	-0.42	0.44	0.02
0.00	0.00	0.00	15.00	0.00	-20.00	-1.30	-0.92	-0.34	15.04	0.65	-18.83	-1.30	-0.92	-0.34	0.04	0.65	1.17
0.00	0.00	0.00	15.00	0.00	0.00	-0.21	-0.68	-0.37	15.04	0.58	0.87	-0.21	-0.68	-0.37	0.04	0.58	0.87
0.00	0.00	0.00	15.00	0.00	20.00	-0.23	-0.41	0.23	15.04	0.57	19.93	-0.23	-0.41	0.23	0.04	0.57	-0.07
0.00	0.00	0.00	-15.00	15.00	-20.00	-0.49	-0.85	-0.03	-16.19	15.83	-23.12	-0.49	-0.85	-0.03	-1.19	0.83	-3.12
0.00	0.00	0.00	-15.00	15.00	0.00	-0.36	-1.38	0.14	-16.10	15.82	-3.37	-0.36	-1.38	0.14	-1.10	0.82	-3.37
0.00	0.00	0.00	-15.00	15.00	20.00	-0.48	-1.84	0.30	-16.19	15.77	15.72	-0.48	-1.84	0.30	-1.19	0.77	-4.28
0.00	0.00	0.00	0.00	15.00	-20.00	-0.62	-0.70	-0.14	-0.42	15.70	-19.03	-0.62	-0.70	-0.14	-0.42	0.70	0.97
0.00	0.00	0.00	0.00	15.00	0.00	-0.75	-0.59	-0.25	-0.43	15.69	0.52	-0.75	-0.59	-0.25	-0.43	0.69	0.52
0.00	0.00	0.00	0.00	15.00	20.00	-0.40	-0.96	-0.05	-0.43	15.76	20.36	-0.40	-0.96	-0.05	-0.43	0.76	0.36
0.00	0.00	0.00	15.00	15.00	-20.00	-0.34	-0.48	-0.04	15.44	16.21	-15.25	-0.34	-0.48	-0.04	0.44	1.21	4.75
0.00	0.00	0.00	15.00	15.00	0.00	-0.86	-0.60	0.06	15.49	16.19	4.51	-0.86	-0.60	0.06	0.49	1.19	4.51
0.00	0.00	0.00	15.00	15.00	20.00	-1.00	-1.51	0.32	15.55	16.11	24.03	-1.00	-1.51	0.32	0.55	1.11	4.03
								average of error				-0.84	-0.77	-0.08	-0.33	0.55	0.51
								standard deviation of error				0.55	0.37	0.27	0.58	0.42	2.70

The average error is within 1 mm in the translation direction and 1 deg in the rotation direction [11]. The standard deviations of the errors are also within 1 mm in the translation direction and within 1 deg in the rotation direction, except for 0γp3. 0αp3 and 0βp3 were used to estimate 0γp3, and the effect of these errors is considered to be reflected in the estimation results. These results indicate that the accuracy is sufficient for a high-precision contact-type 3D position measuring instrument that does not require calibration. In addition, the fact that measurements could be taken immediately after startup indicates that the three-dimensional position-measuring instrument successfully achieved the study's goal of performing highly accurate and large-volume measurements using two commercially available manipulators within a short period.

V. CONCLUSION

This paper stated a three-dimensional position-measuring machine that can quickly perform high-precision And high-volume measurements using two commercially available manipulators. The paper demonstrated how to connect two manipulators utilising a ball joint and proposed a highly accurate measurement theory utilising an IMU. Furthermore, we confirmed that the accuracy of the contact-type three-dimensional position-measuring is within 1 mm on average for translation error, within 1 deg on average for angular error, within 1 mm for the standard deviation of translation error, and 1 deg for

the standard deviation of angular error except for 0γp3, even in the initial state without calibration. This result showed that the method can be used in a neural network to correct estimation errors. To improve the accuracy of the measuring instruments in the future, the following two issues should be addressed:

A. Calibration of Measuring Instrument

The proposed measuring instrument has a unique structure that uses two commercially available manipulators and an IMU. Therefore, a calibration method that is different from conventional methods is required. Consequently, we will devise a new calibration method that considers mechanism errors during machining and assembly, which correspond to internal error parameters, and attachment errors, which correspond to external error parameters, to achieve a more accurate instrument.

B. Calibration at Time of Test Field Installation

Installing the test field in the measurement instrument is necessary to acquire data for the neural network teacher. At that time, an attachment error, an external error parameter, is generated between the pipes in the test field and the measurement device. Since this error significantly impacts the learning process, calibration of the external error parameter is necessary. Therefore, we will develop a method to recalibrate only the external parameters using the aforementioned internal parameters.

DECLARATION STATEMENT

I must verify the accuracy of the following information as the article's author.

- **Conflicts of Interest/ Competing Interests:** Based on my understanding, this article has no conflicts of interest.
- **Funding Support:** This article has not been funded by any organizations or agencies. This independence ensures that the research is conducted with objectivity and without any external influence.
- **Ethical Approval and Consent to Participate:** The content of this article does not necessitate ethical approval or consent to participate with supporting documentation.
- **Data Access Statement and Material Availability:** The adequate resources of this article are publicly accessible.
- **Author's Contributions:** The authorship of this article is contributed solely.

REFERENCES

1. Japan Institute of Wastewater Engineering Technology, "Development foundation survey of sewerage facilities management robot", Sewer New Technology Annual Report of the Institute, 1992, pp.43-52. https://www.jiwet.or.jp/library/research
2. Rome, E., Hertzberg, J., Kirchner, F., Licht, U. and Christaller, T., "Towards Autonomous Sewer Robots: the MAKRO Project", Urban Water, Vol. 1, 1999, pp. 57-70. DOI: https://doi.org/10.1016/S1462-0758(99)00012-6
3. Streich, H. and Adria, O., "Software approach for the autonomous inspection robot MAKRO", in Proceedings of the 2004 IEEE International Conference on Robotics and Automation, 2004, pp. 3411-3416. DOI: https://doi.org/10.1109/ROBOT.2004.1308781
4. Birkenhofer, C., Regenstein, K., Zöllner, J. M. and Dillmann, R., "Architecture of multi-segmented inspection Robot KAIRO-II", DOI: 10.1007/978-1-84628-974-3_35, In book: Robot Motion and Control, 2007, pp.381-389. DOI: https://doi.org/10.1007/978-1-84628-974-3_35
5. Kazutomo, F., Toshikazu, S., Mikio, G., Yoshiki, I. and Hirofumi M., "Miniaturisation of the piping inspection robot by modularisation", 44th Graduation Research Presentation Lecture of Student Members of the JSME, 2014, 613. DOI: https://doi.org/10.1299/jsmecs.2014.52._613-1_
6. Hirofumi M., Ryota, K., "Development of a small autonomous pipe inspection robot (Modularisation of hardware using the technique of wooden mosaic work)", Transactions of the Japan Society of Mechanical Engineers, Vol . 82, No.839, 2016, pp.1-16. DOI: https://doi.org/10.1299/transjsme.15-00635
7. Hirofumi M., "Automatic Compensation of the Positional Error Utilising Localisation Method in Pipe", International Journal of Recent Technology and Engineering (IJRTE), Vol . 9, No.6, 2021, pp.151-157. DOI: https://doi.org/10.35940/ijrte.f5529.039621
8. Hirofumi M., "Impact of Tire Shape on Localisation Accuracy in Piping Inspection Robots", International Journal of Recent Technology and Engineering (IJRTE), Vol . 12, No.6, 2024, pp.35-42. DOI: https://doi.org/10.35940/ijrte.F8016.12060324
9. Hirofumi M., "Real-Time Processing of Localisation for Piping Inspection Robot", International Journal of Research in Academic World (IJRAW), Vol . 3, No.9, 2024, pp.25-31. https://academicjournal.ijraw.com/media/post/IJRAW-3-9-11.1.pdf
10. Hirofumi M., "Calibration Considering the Direction of Rotation for Contact Type Three-Dimensional Position-Measuring Instruments", International Journal of Recent Technology and Engineering (IJRTE), Vol . 12, No.3, 2023, pp.10-19. DOI: https://doi.org/10.35940/ijrte.C7867.0912323
11. Hirofumi M., "A Contact Type Three Dimensional Position Measuring Instrument for Verification of a Piping Inspection Robot", International Journal of Recent Technology and Engineering (IJRTE), Vol . 10, No.6, 2022, pp.65-72. DOI: https://doi.org/10.35940/ijrte.F6840.0310622

AUTHOR'S PROFILE

Hirofumi Maeda is a Professor in the Information Science and Technology Department at the National Institute of Technology (KOSEN), Yuge College. Dr. Maeda's research focuses on the practical application of mechanical engineering, specifically developing rescue robots, pipe inspection robots, and natural language processing systems. Dr. Maeda previously worked as a researcher at the NPO International Rescue System Institute. Dr. Maeda is a member of the Japan Society of Mechanical Engineers, the Robotics Society of Japan, the Japan Association for College of Technology, and the Japan Institute of Marine Engineering. Dr. Maeda has published 16 peer-reviewed papers and presented 85 papers. Additionally, Dr. Maeda received two awards at academic conferences and secured 15 external funding sources.